Structural Engineering and Mechanics, *Vol. 61, No. 1 (2017) 91-103*
DOI: https://doi.org/10.12989/sem.2017.61.1.091

Dynamic behavior of pergola bridge decks of high-speed railways

Jokin Ugarte[*1], Antonio Carnerero[2a] and Francisco Millanes[1,2b]

[1]*IDEAM S.A. 19 Jorge Juan St. 28001, Madrid, Spain*
[2]*Universidad Politécnica de Madrid. E.T.S. de Ingenieros de Caminos, Canales y Puertos, Department of Continuum Mechanics and Structures, 3 Profesor Aranguren St. 28040, Madrid, Spain*

(Received April 3, 2016, Revised October 15, 2016, Accepted October 20, 2016)

Abstract. This paper analyzes the dynamic behavior of the deck of pergola bridges affected by moving loads, specifically high-speed trains. Due to their characteristic advantages, pergola bridges have become a widely used structural typology on high-speed railways. In spite of such wide-spread use, there are few technical bibliographies published in this field. The first part of this paper develops a simple analytical methodology to study the complex dynamic behavior of these double dimensional structures. The second part compares the results obtained by the proposed formulae and the dynamic response obtained with different and gradually more complex FE models. The results obtained by the analytical model are in close agreement with those obtained by the FE models, demonstrating its potential application in the early design stages of this kind of structure.

Keywords: pergola bridge; high-speed rail; dynamic analysis; railway bridge; two dimensional structures; skew angle

1. Introduction

The dynamic response of civil engineering structures that support railway traffic is a classic problem that has been studied since the middle of the 19th century (Willis 1849, Timoshenko 1922). During the second half of the 20th century, theoretical knowledge of these phenomena (Hillerborg 1948, Frýba 1999) afforded the maturity required to develop the first dynamic-aware structural standards (UIC 1979). With the birth of high-speed rail in Japan, and later in Europe, the state of knowledge grew during the last decades of the 20th century. In Europe, this work was carried out by the D-214 Work Group of the ERRI (ERRI-D214-RP9-A 1999, ERRI-D214-RP9-B 1999, leading to the latest European railway standards (I/SC/PS-OM/2298 1997, EN 1991-2 2003, IAPF07 2007).

This development was mainly focused on structures comparable to the simply supported beam, which was the most commonly used structural typology for the first high-speed railways. During the last few decades, the spread of high-speed railway lines has increased the number and complexity of the projected crossings, thus multiplying the structural typologies used to solve them. This tendency is likely to persist into the future (UIC 2010). Much of the recent research on high-speed railway structural dynamics analyzes the behavior of such structures as continuous bridges (Gabaldón, Goicolea *et al.* (2004)), arch bridges (Ju and Lin 2003, Lacarbonara and Colone 2007), or cable-stayed bridges (Yau and Yang 2004, Bruno, Greco *et al.* 2008). Nonetheless, there are still very few studies about the dynamic behavior of bridges with two dimensional geometry. These structural typologies are usually characterized by the relative importance of the transverse behavior, and are increasingly present on high-speed railway lines. In this field it is important to mention studies such as Marchesiello, Fasana *et al.* (1999), (Zhu and Law 2003, Carnerero 2007 or Martínez-Rodrigo, Lavado *et al.* 2010, which analyze different phenomena, all related to the two dimensional nature of some typologies of bridge decks.

The pergola bridge is one of the main structural typologies used on high-speed railway lines that has a marked two dimensional geometry. However, almost no research exists on pergola bridges except for a few studies that refer to particular examples (Goicolea 2007). Thus, this deck typology lacks any treatment by the current standards of dynamic effects on railway structures, leading to time-consuming and sometimes unsecure structural designs.

The aim of this paper is to study the characteristics of the dynamic behavior of pergola bridge decks, and to propose analytical tools that produce deeper understanding. To this end, the paper is organized in two parts. In the first section, the authors propose an analytical methodology for the dynamic analysis of pergola bridge decks. The second part focuses on the numerical verification of the analytical methodology, trying to establish its validity and explain its applications and main restrictions. The final section presents the main conclusions of the paper.

2. Analytical methodology for the dynamic study of pergola bridge decks

As defended in the following section (2.1), the deck of a pergola bridge can be dynamically analyzed by means of a rectangular orthotropic plate simply supported on its four edges. The methodology explained in the current section

*Corresponding author, Ph.D. Student
E-mail: jokin.ugarte@ideam.es
[a]Ph.D., E-mail: antonio.carnerero@upm.es
[b]Ph.D., E-mail: fco.millanes@upm.es

http://www.techno-press.org/?journal=sem&subpage=8 ISSN: 1225-4568 (Print), 1598-6217 (Online)

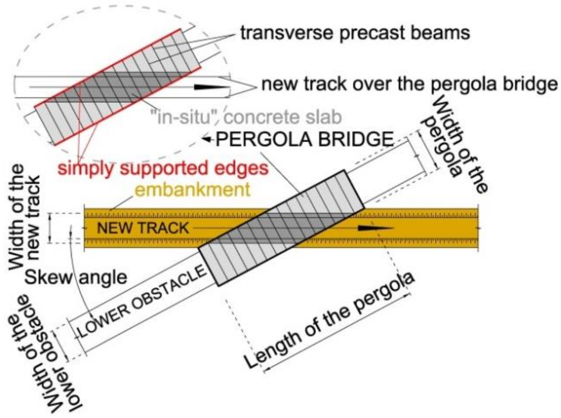

Fig. 1 Left: Pergola bridge on the Spanish high-speed railway network. Right: Diagram of the geometric and structural basis of pergola bridges

analytically resolves the integration of its equation of motion, subjected to the skewed passage of moving loads.

The procedure follows the one proposed in Yang, Yau *et al.* (1997) for integrating the equation of motion of a simply supported beam that is subjected to the passage of moving vehicles. This procedure is also used in Carnerero (2007) and Carnerero, Ripa *et al.* (2014) to integrate the equation of motion of a simply supported rectangular orthotropic plate subjected to the passage of moving loads along the direction of one of its main axes. The current study applies this research to the case of skewed passage of moving loads, which permits application of the analytical methodology to the specific case of pergola bridges characterized by crossings with small skew angles (angle formed between the track to be constructed and the approximately linear obstacle over which the railway is projected to pass), Fig. 1.

The presented methodology is valid for any kind of moving vehicles crossing at any angle over an orthotropic plate simply supported along its four edges. The paper is focused on the skewed passage of high-speed railway trains over the most frequently used pergola bridge deck typology: precast transverse beams spanning the direction of the short edge topped by an *in-situ* concrete slab (Fig. 1).

2.1 Modelization of a pergola bridge deck by an orthotropic plate simply supported on its four edges

To develop the analytical model, the deck of a pergola bridge was conceptualized by an orthotropic plate simply supported along its four edges. This conceptualization was based on reasoned simplifications that were later analyzed and checked by FE numerical models (section 3). Note the following simplifications:

Support of the short edges: The short edges of a pergola bridge deck are free. However, to simplify the formulation of the modal shapes of the deck, the authors decided to simply support them.

Uniform distribution of the mass: On the deck of a pergola bridge, the mass coming from the track (whether ballasted or not) concentrates in a narrow band around the actual track (henceforth referred to as "central band"). However, the proposed analytical methodology considers the mass to be uniformly distributed over the total surface of the deck. Therefore, for the development of the analytical method the mass per unit surface of the whole deck was assumed to be identical to the mass per unit surface of the central band.

Slab over the entire deck surface: Although this is common on some pergola bridges, usually the concrete slab tends to cover only the minimum surface necessary. This approximately coincides with the central band. For the same reasons mentioned in the previous point, the analytical methodology supposes the slab to be continuous over the entire deck surface.

2.2 Theoretical basis

The theoretical principles of the orthotropic plate are well known and explained in Cusens and Pama (1975), Manterola (1977) or Arenas (1981). The main characteristics of the rectangular orthotropic plate are summarized here

$$D_x = \nu^2 \cdot \frac{E_{slab}}{1-\nu^2} \cdot \frac{e^3}{12} + \frac{E_{beam} \cdot I_{x,0}}{s_y} \tag{1}$$

$$D_y = \nu^2 \cdot \frac{E_{slab}}{1-\nu^2} \cdot \frac{e^3}{12} + \frac{E_{beam} \cdot I_{y,0}}{s_x} \tag{2}$$

$$D_1 = D_2 = \nu \cdot \frac{E_{slab}}{1-\nu^2} \cdot \frac{e^3}{12} \tag{3}$$

$$D_{xy} = \frac{G_{slab} \cdot e^3}{6} + \frac{G_{beam} \cdot J_x}{s_y} \tag{4}$$

$$D_{yx} = \frac{G_{slab} \cdot e^3}{6} + \frac{G_{beam} \cdot J_y}{s_x} \tag{5}$$

The equation of motion of the orthotropic plate can be found in Frýba (1999) or Carnerero (2007), and it is represented in Eq. (7).

$$m(x,y) \cdot \frac{\partial^2 v(x,y,t)}{\partial t^2} + c(x,y) \cdot \frac{\partial v(x,y,t)}{\partial t} + D_x \cdot \frac{\partial^4 v(x,y,t)}{\partial x^4} + 2H \cdot \frac{\partial^4 v(x,y,t)}{\partial x^2 \cdot \partial y^2} + D_y \cdot \frac{\partial^4 v(x,y,t)}{\partial y^4} = p(x,y,t) \tag{7}$$

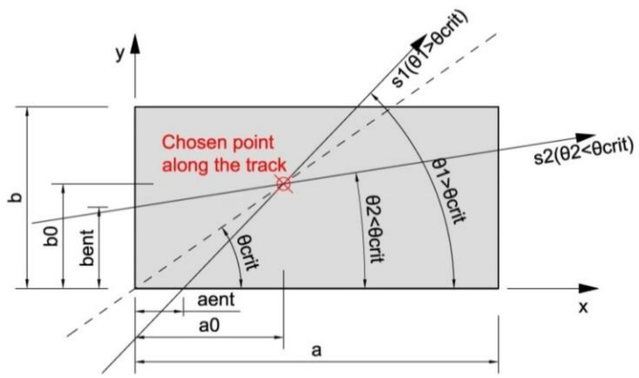

Fig. 2 Geometric parameters of a pergola bridge deck considered in the analytical methodology

For clarity, Appendix A lists and explains the parameters presented in the previous equation, as well as all other parameters included in this paper.

The mentioned bibliography solves the frequency equation for the case in which the four edges of the plate are simply supported, producing the following modal shapes and vibration frequencies (Fig. 2 presents the geometric parameters)

$$\phi_r(x,y) = \sin\left(\frac{n\cdot\pi}{a}\cdot x\right)\cdot\sin\left(\frac{m\cdot\pi}{b}\cdot y\right) \tag{8}$$

$$w_r = \pi^2\cdot\sqrt{\frac{\left[D_x\cdot\frac{n^4}{a^4}+2\cdot H\cdot\frac{n^2\cdot m^2}{a^2\cdot b^2}+D_y\cdot\frac{m^4}{b^4}\right]}{m}} \tag{9}$$

2.3 Integration of the equation of motion for a single moving load

Fig. 2 presents the geometric parameters of the deck of a pergola bridge considered in the analytical methodology. The track along which vehicles cross the deck is assumed to be linear, and s denotes the position coordinate along the track. In Fig. 2, s_1 and s_2 show two different track possibilities in which the vehicles enter the deck from its long and short edges, respectively. The main parameters in Fig. 2 are defined in Notation.

This study is focused on pergola bridge decks when moving loads enter the decks at the long edges. The proposed analytical methodology can also be applied to instances where moving loads enter decks at the short edges, but not to cases where moving loads enter the deck at the long edge and leave through the short edge, and vice versa. The mathematical formulae could be modified to include these particular cases, but the increased mathematical complexity this would cause, as well as a lack of interest in these cases, led the authors to exclude them during the preliminary research stages. This applies to other analytically definable track geometries, such as a circular alignment.

Using the geometric parameters previously defined and the Heaviside step function, the position of one load of P value that enters the deck at the temporal origin is defined at any instant on the global coordinates by the following expressions

$$x = s(v,t)\cdot\cos\theta + \left(a_0 - \frac{b_0}{\tan\theta}\right)\cdot H(\theta-\theta_{crit}) \tag{10}$$

$$y = s(v,t)\cdot\sin\theta + (b_0 - a_0\cdot\tan\theta)\cdot H(\theta_{crit}-\theta) \tag{11}$$

Where $s(v,t)$ refers to the position of the load along the track once it enters the deck. Hence, the modal shapes of the deck can be expressed only in terms of a single spatial parameter, $s = s(v,t)$.

$$\begin{aligned}\phi(x,y) = \phi\Bigg(& s\cdot\cos\theta + \left(a_0 - \frac{b_0}{\tan\theta}\right)\cdot H(\theta-\theta_{crit}),\\ & s\cdot\sin\theta + (b_0 - a_0\cdot\tan\theta)\\ & \cdot H(\theta_{crit}-\theta)\Bigg)\end{aligned} \tag{12}$$

Due to the time-space dependency ($s = v\cdot t$), the generalized load can be obtained by means of the Dirac function

$$\begin{aligned}P_r^* = \iint_0^{a,b}\Big[&\sin\left(\frac{n\cdot\pi}{a}\cdot x\right)\cdot\sin\left(\frac{m\cdot\pi}{b}\cdot y\right)\cdot P\cdot\delta(s-v\cdot t)\Big]\\ &\cdot dx\cdot dy\end{aligned} \tag{13}$$

$$\begin{aligned}P_r^* &= P\cdot H(\Delta t - t)\\ &\cdot\left[\sin\left(\frac{n\cdot\pi}{a}\cdot\left(v\cdot t\cdot\cos\theta + \left(a_0-\frac{b_0}{\tan\theta}\right)\cdot H(\theta-\theta_{crit})\right)\right)\right.\\ &\left.\cdot\sin\left(\frac{m\cdot\pi}{b}\cdot\left(v\cdot t\cdot\sin\theta + (b_0 - a_0\cdot\tan\theta)\cdot H(\theta_{crit}-\theta)\right)\right)\right]\end{aligned} \tag{14}$$

Contrary to what happens when a punctual load passes over a simply supported beam (Yang, Yau *et al.* 1997) and passes longitudinally over an orthotropic plate (Carnerero 2007), the resulting generalized load is not a harmonic load. In the cases studied in the references, the temporal discontinuity of the generalized load can be eliminated using a fictitious load (Yang, Yau *et al.* 1997), and the equation of motion directly integrated.

In the case study, the skewed passage of the punctual load forces consideration of the double curvature of the deck, and so the generalized load becomes the product of two harmonic loads. This is the first and main methodological difference between the mentioned references and the analytical solution presented in this paper. Notice that if the skew angle is assumed to be equal to 0 (longitudinal passage), the second harmonic in Eq. (14) becomes constant, achieving the particular case studied in Carnerero (2007) and Yang, Yau *et al.* (1997). In the case of a skewed passage, a prior step is needed that becomes the generalized load of P amplitude in a sum of two harmonic loads with $P/2$ amplitude. The mathematical operation that allows this conversion is the following basic trigonometric principle

$$\sin(A)\cdot\sin(B) = \frac{\cos(A-B)-\cos(A+B)}{2} \tag{15}$$

Taking into account that the sine and the cosine functions are related by $\cos(A) = \sin(A + 90º)$, the

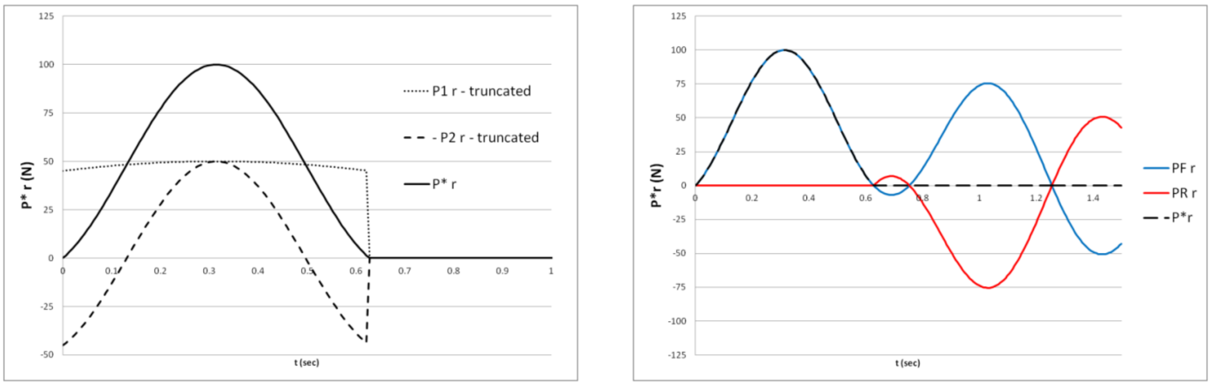

Fig. 3 Left: Composition of the generalized load as the sum of two truncated harmonic loads; Right: Composition of the generalized load as the sum of four non-truncated harmonic loads

following generalized load expression can easily be derived

$$\begin{aligned} P_r^* &= \frac{P}{2} \cdot H(\Delta t - t) \\ &\Big[\sin\Big(v \cdot \pi \cdot \Big(\frac{n}{a} \cdot \cos\theta - \frac{m}{b}\sin\theta\Big) \cdot t + \frac{n \cdot \pi}{a} \\ &\cdot \Big(a_0 - \frac{b_0}{\tan\theta}\Big) \cdot H(\theta - \theta_{crit}) - \frac{m \cdot \pi}{b} \cdot (b_0 - a_0 \cdot \tan\theta) \\ &\cdot H(\theta_{crit} - \theta) + \frac{\pi}{2}\Big) - \sin\Big(v \cdot \pi \cdot \Big(\frac{n}{a} \cdot \cos\theta + \frac{m}{b}\sin\theta\Big) \\ &\cdot t + \frac{n \cdot \pi}{a} \cdot \Big(a_0 - \frac{b_0}{\tan\theta}\Big) \cdot H(\theta - \theta_{crit}) + \frac{m \cdot \pi}{b} \\ &\cdot (b_0 - a_0 \cdot \tan\theta) \cdot H(\theta_{crit} - \theta) + \frac{\pi}{2}\Big) \end{aligned} \tag{16}$$

The previous expression can be seen as the combination of two different harmonic loads, truncated once the real load leaves the deck by the Heaviside function $H(\Delta t - t)$ (Fig. 3, left).

$$P_r^* = P1_{r,trunc.} - P2_{r,trunc.} \tag{17}$$

$$\begin{aligned} P1_{r,trunc.} &= \frac{P}{2} \cdot H(\Delta t - t) \cdot sin\Big(v \cdot \pi \cdot \Big(\frac{n}{a} \cdot cos\,\theta - \\ &\frac{m}{b} sin\,\theta\Big) \cdot t + \frac{n \cdot \pi}{a} \cdot \Big(a_0 - \frac{b_0}{tan\,\theta}\Big) \cdot H(\theta - \theta_{crit}) \\ &- \frac{m \cdot \pi}{b} \cdot (b_0 - a_0 \cdot tan\,\theta) \cdot H(\theta_{crit} - \theta) + \frac{\pi}{2}\Big) \end{aligned} \tag{18}$$

$$\begin{aligned} P2_{r,trunc.} &= \frac{P}{2} \cdot H(\Delta t - t) \cdot sin\Big(v \cdot \pi \cdot \Big(\frac{n}{a} \cdot cos\,\theta \\ &+ \frac{m}{b} sin\,\theta\Big) \cdot t + \frac{n \cdot \pi}{a} \cdot \Big(a_0 - \frac{b_0}{tan\,\theta}\Big) \cdot H(\theta - \theta_{crit}) \\ &+ \frac{m \cdot \pi}{b} \cdot (b_0 - a_0 \cdot tan\,\theta) \cdot H(\theta_{crit} - \theta) + \frac{\pi}{2}\Big) \end{aligned} \tag{19}$$

The last step that enables the direct integration of the equation of motion is to eliminate the time discontinuity that truncates the defined two harmonic loads once the real load leaves the deck. First, truncation of the two defined harmonic loads is eliminated, achieving two infinite harmonic loads ($P1_r$ and $P2_r$) whose combination achieves the non-truncated generalized load that is going to be defined as front load (PF_r). Then, the effect of the front load over the deck once the real load leaves the structure is eliminated by a fictitious load defined as rear load (PR_r), equal and opposite in sign to the front load, that begins to act at the same instant the real load leaves the deck. The rear load is composed of two other harmonic functions that eliminate $P1_r$ and $P2_r$ and are defined as $P3_r$ and $P4_r$ respectively. Thus, the generalized load can be stated as the composition of the front and the rear loads.

$$P_r^* = PF_r + PR_r \tag{20}$$

$$PF_r = P1_r + (-P2_r) \tag{21}$$

$$PR_r = P3_r + (-P4_r) \tag{22}$$

Fig. 3 describes the mathematical mechanism for the definition of the generalized load (P_r^*) by two truncated harmonic loads (left) and by four non-truncated harmonic loads (right).The generalized load is represented for the particular case of the first vibration mode of a deck with the following characteristics:

Dimensions: $a = 20\ m$ y $b = 10\ m$.

• Passage speed: $v = 100\ km/h$.

• Position of a singular point along the track and skew angle: centered on the deck and $\theta = 35º$.

• Value of the single punctual load: $P = 100\ N$.

The definition of these four harmonic loads takes the following shape

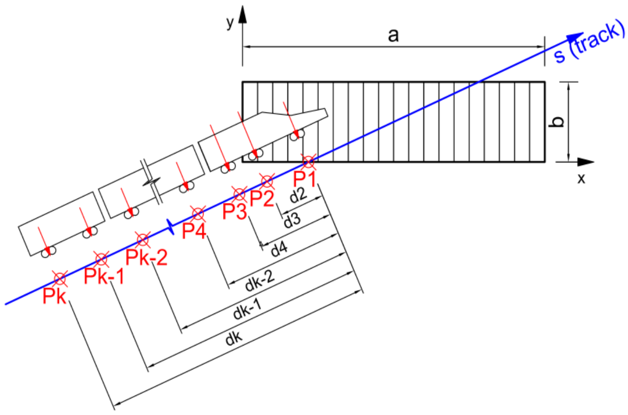

Fig. 4 Sketch of the train of loads and distance of each load to the spatial origin-Plan view and folded train elevation

$$Pi_r = \frac{P}{2} \cdot \sin\left(w_{P\mathrm{i},r} + \varphi_{Pi,r}\right) \tag{23}$$

Appendix A defines the circular frequency and the phase angle of each of the four harmonic loads that form the generalized load.

This is the second methodological difference between the analytical methodology proposed in this paper and the methodology presented in Carnerero (2007), Yang, Yau *et al.* (1997). In these references, due to the definition of the front load by a single harmonic, it is possible to maintain the phase angle of the rear load equal to the phase angle of the front load (both equal to 0) by the explicit definition of the sign of the rear load related to the number of the vibration mode: $P_r^* = PF_r + (-1)^{n+1} \cdot PR_r$. This method cannot be used in the current case, and this is why the phase angle of the two harmonic functions of the rear load need to be defined as described in Eq. (A.7) and Eq. (A.8). On the other hand, the methodology proposed in this paper can be used in both cases presented in Yang, Yau *et al.* (1997), Carnerero (2007), and so, it can be seen as a generalization of the methodology used in the mentioned references.

Once the generalized load is formed by four independent harmonic loads by means of the superposition principle, their effect over the structure can be obtained as the superposition of the effects of each one of them. Integrating a system with a single degree of freedom (in this case, each vibration mode) is a well-known dynamic problem described in Clough and Penzien (1995). However, it must be remarked that the existence of a phase angle on the harmonic loads slightly changes the definition of the integration constants to those of the basic case. By means of the modal superposition method and the mathematic tools previously mentioned, the vertical displacement of any point of a deck subjected to the skewed passage of a single moving load can be defined as the following time dependent function

$$v_r(x,y,t) = \sum_{r=1}^{R} \left[\frac{\sin\left(\frac{n \cdot \pi}{a} \cdot x\right) \cdot \sin\left(\frac{m \cdot \pi}{b} \cdot y\right)}{K_r^*} \cdot \frac{P}{2} \cdot \left[\frac{A_r(t) + C_r(t) \cdot H(t - \Delta t)}{\left(1 - {\beta_{1,r}}^2\right)^2 + \left(2 \cdot \xi_r \cdot \beta_{1,r}\right)^2} - \frac{B_r(t) + D_r(t) \cdot H(t - \Delta t)}{\left(1 - {\beta_{2,r}}^2\right)^2 + \left(2 \cdot \xi_r \cdot \beta_{2,r}\right)^2} \right] \right] \tag{24}$$

$A_r(t)$, $B_r(t)$, $C_r(t)$ and $D_r(t)$ are temporal functions used to simplify the general formulae. Appendix B defines these functions for the case of Eq. (25).

2.4 Generalization for a train of moving loads

Generalization of the results presented in the previous section is easily achievable using the superposition principle for a moving train of loads. Therefore, the effect of each load can be obtained independently and later superposed. However, some considerations must be taken into account.

On one hand, some new parameters need to be defined: the relative distance of each single load to a common spatial origin, and the different values of each load. Using the distance along the track from each load to a common spatial origin and the distance from that to the beginning of the structure, one can easily define the instant when each load enters and then leaves the deck. Usually, it is best to define the spatial origin of the first load of the train along with the time that this first load enters the deck. The speed of the train of loads is considered to be constant, which is quite reasonable for the common lengths of high-speed pergola bridges.

In this way, the vertical displacement of any of the points of a deck subjected to the skewed passage of a moving train of loads can be defined as a time dependent function as follows

$$v(x,y,t) = \sum_{r=1}^{R} \frac{\sin\left(\frac{n \cdot \pi}{a} \cdot x\right) \cdot \sin\left(\frac{m \cdot \pi}{b} \cdot y\right)}{K_r^*} \cdot \sum_{k=1}^{KP} \frac{P_k}{2} \cdot \left[\frac{A_{rk}(t) \cdot H(t - t_k) + C_{rk}(t) \cdot H(t - t_k - \Delta t)}{\left(1 - {\beta_{1,r}}^2\right)^2 + (2 \cdot \xi_r \cdot \beta_{1r})^2} - \frac{B_{rk}(t) \cdot H(t - t_k) + D_{rk}(t) \cdot H(t - t_k - \Delta t)}{\left(1 - {\beta_{2,r}}^2\right)^2 + \left(2 \cdot \xi_r \cdot \beta_{2,r}\right)^2} \right] \tag{25}$$

Finally, Appendix B lists the definition of the temporal functions mentioned in the previous section. Note that the rest of the dynamic parameters of the deck (velocity and acceleration) can easily be obtained by the time derivation of the mentioned temporal functions, while Eq. (25) remains unchanged. Their resolution is elementary, which is why they are not represented here.

3. Numerical simulation of a pergola bridge deck by FEM: validation and main limitations of the analytical methodology

This section discusses the validity of the proposed analytical methodology to represent the dynamic behavior of pergola bridge decks, and to analyze its main limitations by comparison to gradually more complex numerical FE models.

The assessment begins with a comparison of the analytical model (AM) and an equivalent numerical model (NMT0), which validates the analytical formulae. Then, the influence of the support of the short edges is analyzed, comparing the NMT0 (simply supported on its four edges) and the NMT1 (simply supported only along its long edges). Finally, we present three different models that represent real types of pergola bridge decks (NMT2, NMT3 and NMT4) and compare them to the analytical model (AM). This is done to assess the validity of the proposed analytical methodology to simulate the real dynamic behavior of a pergola bridge deck.

This section begins with a brief summary of the analyzed numerical models. Next, the characteristics of the numerical dynamic analysis are stated, ending the section with a comparison of the dynamic results obtained from the

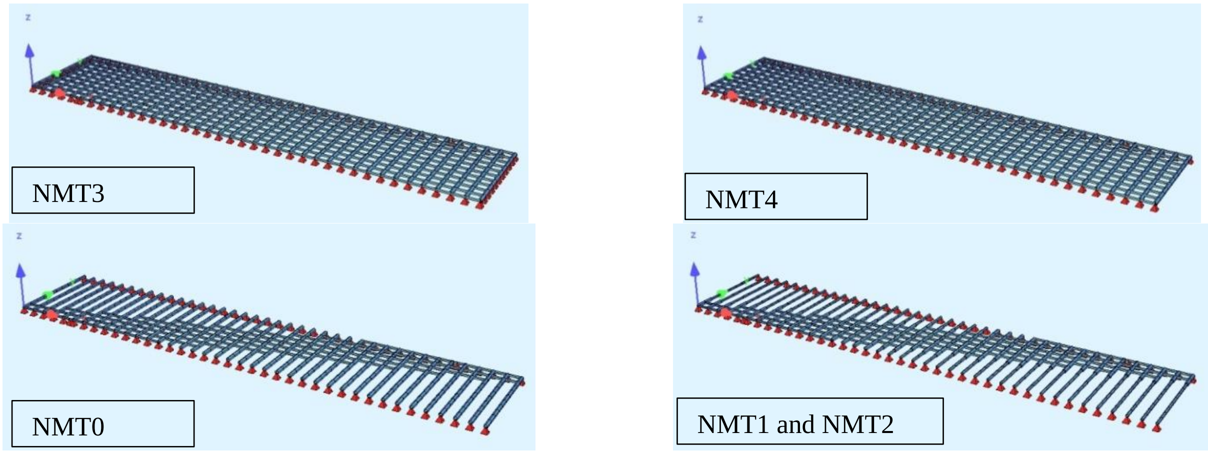

Fig. 4 From left to right and from top to bottom NMT0, NMT1 and NMT2 (represented by the same model with different mass distributions), NMT3 and NMT4

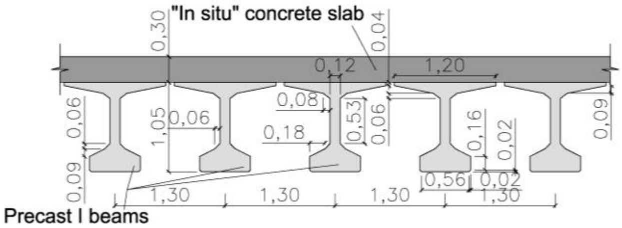

Fig. 5 Cross section of the analyzed deck of a pergola bridge

different models studied.

3.1 Analyzed numerical models

Numerical model type 0 (NMT0): This numerical model is equivalent to the proposed analytical model (AM), and therefore represents the same reality. The short edges are simply supported, and the mass and the slab uniformly distributed. It tries to validate the functioning of the AM.

Numerical model type 1 (NMT1): This represents the NMT0 in which the support of the short edges has been eliminated. It attempts to analyze the influence of the support on the short edges.

Numerical model type 2 (NMT2): This represents the NMT1 in which the mass has been concentrated on the central band. It tries to analyze the influence of the non-uniform distribution of the vibrating mass. The NMT2 represents the real situation of a pergola bridge deck in which the concrete slab is distributed over the total deck surface.

Numerical model type 3 (NMT3): This represents the NMT2 in which the slab has been concentrated on the central band. In spite of it, the bending inertia of the transverse beams remains constant. It attempts to analyze the influence of the longitudinal stiffness of the slab outside the central band. The NMT3 represents the real situation of a pergola bridge deck in which the longitudinal continuity of the slab has been eliminated, maintaining a certain width of the slab over each transverse precast beam and thus, their bending inertia.

Numerical model type 4 (NMT4): This represents the NMT3 where outside the central band the bending inertia of the model's transverse bars is reduced to the bending inertia of the precast beams. It tries to analyze the effect of the loss of transverse stiffness of the deck caused by eliminating the slab over the transverse beams. The NMT4 represents the most common pergola bridge deck typology in which the *in-situ* slab is concentrated on the central band.

In all cases, the numerical simulation of a pergola bridge deck has been carried out by means of grillage models Hambly (1991). Fig. 4 represents the studied FE models.

3.2 Modelization and definition of the parameters involved

A standard pergola bridge deck is used for the numerical analysis. It has been pre-dimensioned using general design rules. It is supposed to be a deck 20 m width (b) and 100 m long (a), formed with 1.05 m height (h) precast I beams topped by a 0.30 m slab (e). Thus, the span to height ratio b/h is 14.81, a typical value for railway bridges. The skew angle of the rail and the main beams (θ) is 15º, a common value for pergola bridges. This angle is in good correlation with the length to width ratio of the deck ($a/b = 5$). The separation between transverse beam axes (s) is 1.30 m, which is a low value typical for I beams in this kind of structures. Fig. 6 represents the cross section of the assessed deck, showing its main geometrical parameters.

As mentioned before, grillage models were used for the numerical simulation of a pergola bridge deck. The longitudinal bars of the grillage represent the slab of the deck, while the transverse bars represent the transversal composed beams, formed by the composition of the precast beams and the *in-situ* concrete slab, as shown on the figure 7. The longitudinal and the transverse bars are placed on the same plane, linked to their corresponding gravity centers.

The table below presents the main geometric and mechanical characteristics of the different analytical and numerical models. The concrete compressive strength in cylindrical, standardized samples is assumed to be 50 MPa for the precast beams and 30 MPa for the *in-situ* slab. The bars of the numerical models are homogenized to 50 MPa

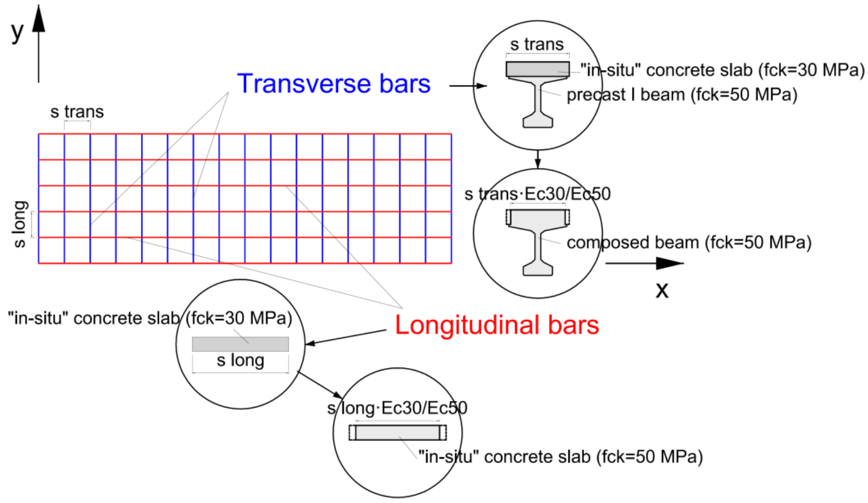

Fig. 6 Explicative sketch of the numerical FE grillage models

Table 1 Mechanical characteristics of the NM

I_{trans} (m^4)	J_{trans} (m^4)	$I_{long.}$ (m^4)	$J_{long.}$ (m^4)	$m_{trans.}$ (kg/m)	$m_{long.\ slab}$ (kg/m)	$m_{long.ballast}$ (kg/m)
0.266/0.1078	0.015/0.0052	0.0039	0.0078	1732	1500	1800

Table 2 Geometric and mechanical characteristics of the AM

a (m)	*b* (m)	θ (º)	$I_{trans.}$ (m^4)	$S_{trans.}$ (m)	$J_{trans.}$ (m^4)	*e* (m)	*m* (kg/m^2)
100	20	15	0.1330	1.3	0.00266	0.3	2325

Table 3 Geometric characteristics of the NM

a (m)	*b* (m)	θ (º)	$S_{trans.}$ (m)	*e* (m)	$S_{long.}$ (m)
98.8	*20*	15	*2.60*	0.3	2.00

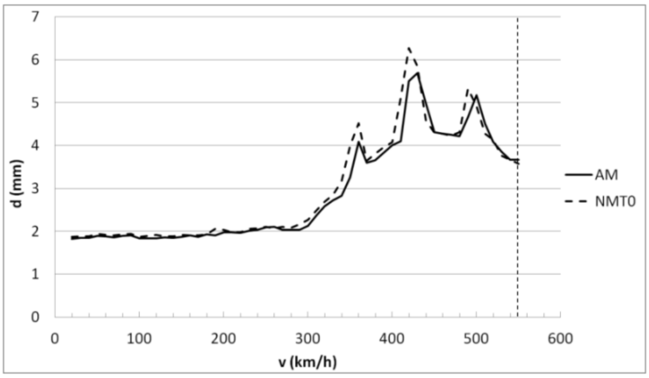

Fig. 7 Displacement response on the center of the deck for the TALGO AV passing over the AM and the NMT0

concrete, consequently adapting the width of the slab (Fig. 7). The elastic modulus of the concrete is considered to be $E_c = 1.175 \cdot 8500\sqrt[3]{f_{ck}+8}$, and its density 2500 kg/m^3 (EN 1992-1-1 (2004)). The density of the ballast is considered to be 1800 kg/m^3 (IAPF-07 2007).

In Table 3 two values are defined for the bending and torsional inertia of the main beams, separated by an inclined bar (“value 1”/“value 2”). “Value 1” defines the value of the parameter for the composed beam, while “value 2” defines the value of the parameter for the precast beam alone.

In order to reduce the numerical complexity of the FE models, the distance between the axes of the transverse beams is increased to the double on the numerical models, increasing accordingly their mechanical characteristics. As explained in reference Ugarte (2013), this variation does not affect the dynamic behavior of the AM and so, the results are totally equivalent.

On the following paragraphs, the dynamic parameters of the developed analysis are described. As stated in the previous section, the proposed analytical methodology was developed using the modal superposition method. Its dynamic results were obtained by using its first 56 vibration modes. The frequency limit considered in the analysis was 30 Hz, as stated by the Spanish and European standards EN 1991-2 (2003), IAPF-07 (2007). Thirty-one of these vibration modes respond to mode shapes of a single transverse curvature, and 25 of them to mode shapes of a double transverse curvature. However, it must be taken into account that even vibration modes do not excite the evaluated point, situated on the center of the deck. In this way, only 16 vibration modes (odd vibration modes with a single transversal curvature) influence the dynamic behavior of the deck at the studied position.

On the other hand, SOFISTIK, the FE commercial program used to study the numerical models, develops a step-by-step integration method based on the Newmark Beta methods. In this case, two main parameters must be taken into account: frequency limitation and time step length. The time step length for which the Newmark Beta methods are stable is $h \le T \cdot \frac{\sqrt{3}}{\pi}$. The minimum required period (T) corresponds to the highest frequency of the analyzed frequency range, in this case 30 Hz. To achieve a reliable accuracy, the utilized time step length was set at

Table 4 TALGO AV train as defined in IAPF-07 (2007)

d_k (m)	P_k (kN)	d_k (m)	P_k (kN)	d_k (m)	P_k (kN)	d_k (m)	P_k (kN)
0	170	93.8	170	183.49	170	277.29	170
2.65	170	106.94	170	186.14	170	290.43	170
11	170	120.08	170	194.49	170	303.57	170
13.65	170	133.22	170	197.14	170	316.71	170
19.13	170	146.36	170	202.62	170	329.85	170
28.1	170	155.33	170	211.59	170	338.82	170
41.24	170	160.8	170	224.73	170	344.29	170
54.38	170	163.45	170	237.87	170	346.94	170
67.52	170	171.8	170	251.01	170	355.29	170
80.66	170	174.45	170	264.15	170	357.94	170

d_k: Distance from load axis P_k to first load axis (P_1) in m
P_k: Value of the load of axis k in kN

Table 5 Main dynamic parameters of the displacement and acceleration response on the center of the deck for the TALGO AV passing over the AM and the NMT0

Model	$d_{\max}$ (mm)	$v_{d,\max}$ (km/h)	$d_{\max}/d_{static}$	$a_{\max}$ (m/s^2)	$v_{a,\max}$ (km/h)
AM	5.68	430.00	3.11	17.34	500.00
NMT0	6.27	420.00	3.36	17.32	500.00
AM error (%)	-9.32	+2.38	-7.30	+0.10	0.00

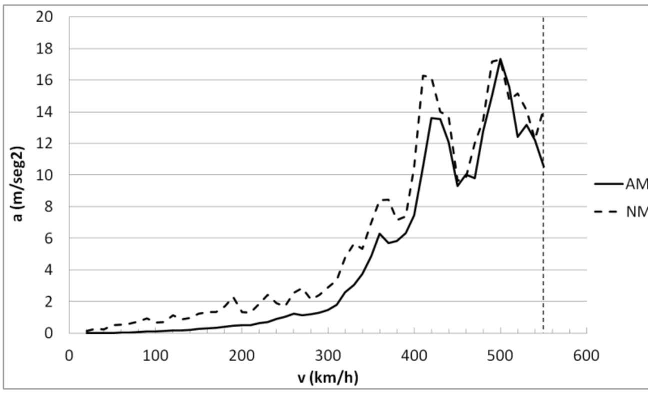

Fig. 8 Acceleration response on the center of the deck for the TALGO AV passing over the AM and the NMT0

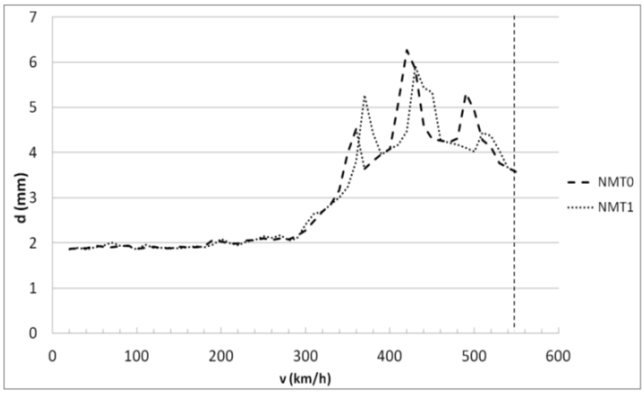

Fig. 9 Displacement response on the center of the deck for the TALGO AV passing over the NMT0 and the NMT1

$h \leq \frac{1}{30Hz} \cdot \frac{1}{\pi} = 0.01061\ sec$. The frequency limitation was made using the Rayleigh damping formulae. The relative damping stated on the Spanish and European standards (EN 1991-2 2003, IAPF-07 2007) for concrete structures ($\xi = 0.02$) was applied to the frequency of the first vibration mode of each numerical model and to the highest frequency of the studied range (30 Hz). This ensured that the relative damping of the frequency range under analysis was lower than the normative one, and that vibration modes with frequencies over 30 Hz did not influence the dynamic behavior of the structure (due to their comparatively high damping). In most cases, the relative damping of the vibration modes within the studied range were very similar to the reference damping.

The vehicle for this study was a train of moving punctual loads. The train used to compare the dynamic results of the different models is the TALGO AV, described in reference IAPF-07 (2007).

3.3 Dynamic analysis

3.3.1 Validation of the analytical model

Figs. 8 and 9 represent the results of the dynamic assessment of the passage of a TALGO AV train over the AM and the NMT0. The analyzed velocity range was 20 km/h to 550 km/h with 10 km/h steps. The evaluation point was set at the center of the deck.

In Figs. 8 and 9, one may observe a good correlation between the AM and the equivalent NMT0. The following table summarizes the main results.

As can be seen, the general dynamic response of the AM is strongly similar to the one of the equivalent NM (NMT0). The achieved error is for most parameters lower than 5%. The maximum displacement obtains a slightly higher error, yet still lower than 10%. The error of the maximum displacement to the static displacement ratio (the impact coefficient) remains between 5-10%.

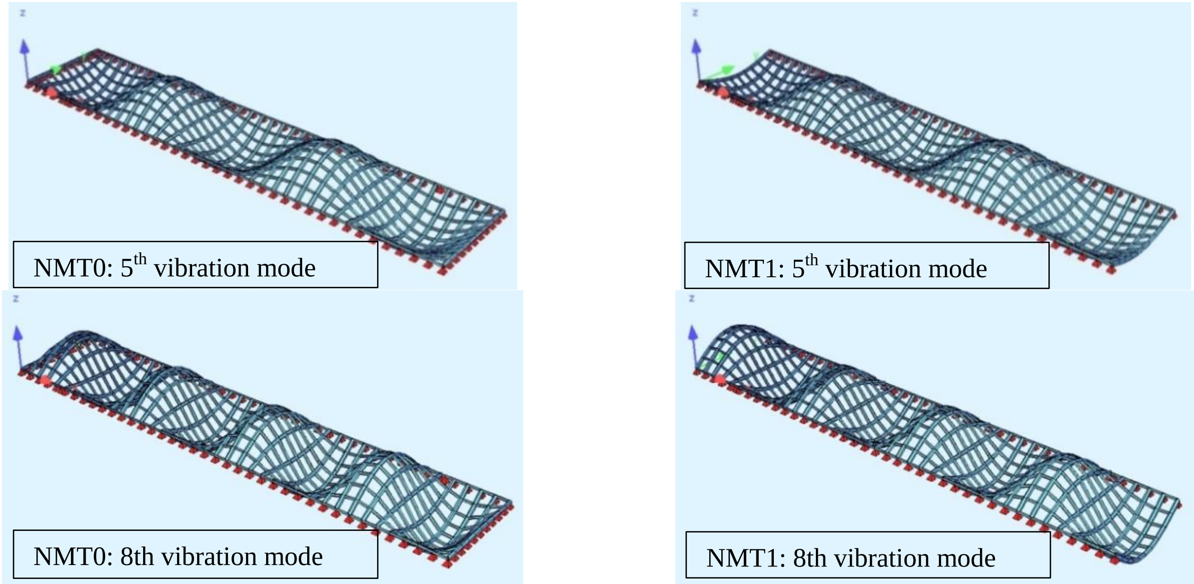

Fig. 10 Mode shapes of the 5th and the 8th vibration modes of the NMT0 and the NMT1, respectively

Table 6 Main dynamic parameters of the displacement and acceleration response on the center of the deck for the TALGO AV passing over the NMT0 and the NMT1

Model	$d_{\max}$ (mm)	$v_{d,\max}$ (km/h)	$d_{\max}/d_{static}$	$a_{\max}$ (m/s^2)	$v_{a,\max}$ (km/h)
NMT0	6.27	420.00	3.36	17.32	500.00
NMT1	5.91	430.00	3.18	17.99	430.00
NMT0 error (%)	+5.99	-2.33	+5.76	-3.72	+16.28

The dynamic parameters involved in design obtained errors below or very similar to 5%, and the general response of the deck is practically identical in both cases. The authors consider that this confirms the validity of the analytical methodology proposed in the previous section.

3.3.2 Evaluation of the influence of the support of the short edges

Figs. 10 and 11 represent the results of the dynamic assessment of the passage of a TALGO AV train over the NMT0 and the NMT1. The analyzed velocity range was 20 km/h to 550 km/h with 10 km/h steps. The evaluation point was set at the center of the deck.

From Figs. 10 and 11, one may conclude that the general dynamic behavior is almost equal in both cases. If the modal shapes of the vibration modes of both models are compared, the similarity is clearly visible, showing that the shape along the track is almost equivalent.

The table below shows the summarized results of the dynamic analysis shown in Fig. 9 and Fig. 11.

Table 6 shows clearly the minor influence the support of the short edges had on the dynamic behavior of the deck. In general, the achieved error is less than or nearly equal to 5%, including the impact factor. The only parameter with a slightly greater error is the resonant velocity for the maximum acceleration. Nevertheless, as can be seen in Fig. 11, there are two resonant peaks for accelerations in both NMT0 and NMT1, with very similar shape and maximum values. The difference in the resonant velocity is determined by small differences in which of the peaks is more relevant on each model. This way, the low influence of the support of the short edges is considered to be confirmed.

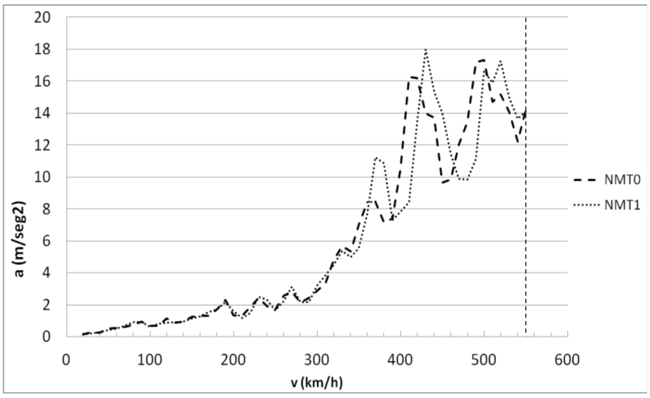

Fig. 11 Acceleration response on the center of the deck for the TALGO AV passing over the NMT0 and the NMT1

3.3.3 Evaluation of the validity of the Analytical Model to represent the deck of a pergola bridge

As mentioned before, models NMT2 to NMT4 represent different construction typologies of pergola bridge decks formed by precast transverse beams that are topped by an *in situ* concrete slab. The differences between these models are based on different distributions of mass and stiffness. Next, the dynamic analyses of the three numerical models are carried out by comparing their dynamic behaviors to the one obtained for the AM.

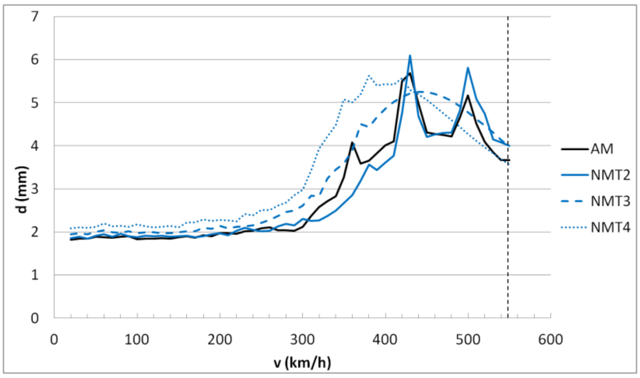

Fig. 12 Displacement response on the center of the deck for the TALGO AV passing over the AM, the NMT2, the NMT3 and the NMT4

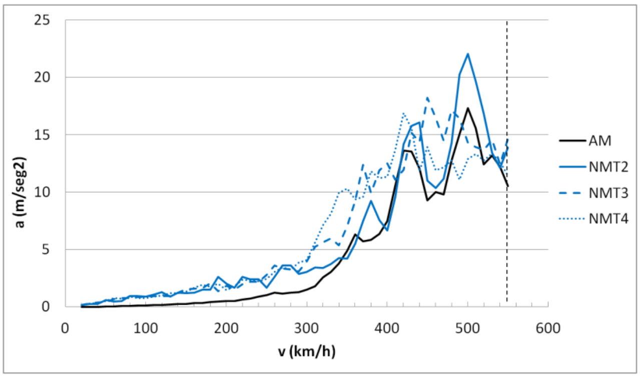

Fig. 13 Displacement response on the center of the deck for the TALGO AV passing over the AM, the NMT2, the NMT3 and the NMT4

Table 7 Main dynamic parameters of the displacement and acceleration response on the center of the deck for the TALGO AV passing over the AM, the NMT2, the NMT3 and the NMT4

Model	$d_{\max}$ (mm)	$v_{d,\max}$ (km/h)	$d_{\max}/d_{static}$	$a_{\max}$ (m/s^2)	$v_{a,\max}$ (km/h)
AM	5.68	430.00	3.11	17.34	500.00
NMT2	6.10	430.00	3.28	22.04	500.00
NMT3	5.25	450.00	2.69	18.24	450.00
NMT4	5.63	380.00	2.71	16.88	420.00
AM to NMT2 error (%)	-6.76	0.00	-5.04	-21.34	0.00
AM to NMT3 error (%)	+8.31	-4.44	+15.65	-4.95	+11.11
AM to NMT4 error (%)	+1.03	+13.16	+15.07	+2.71	+19.05

Figs. 13 and 14 represent the results of the dynamic assessment of the passage of a TALGO AV train over the AM, the NMT2, the NMT3 and the NMT4. The analyzed velocity range was 20 km/h to 550 km/h with 10 km/h steps. The evaluation point was set at the center of the deck.

In spite of the significant differences in mass and stiffness istributions between the analyzed models, the general shape of the dynamic behavior remains very similar. To better understand the specific characteristics of each model and their main differences, the table below shows the summarized results of the dynamic analysis illustrated in Fig. 12 and Fig. 14.

The results shown in Table 7 permit the extraction of the following conclusions:

NMT2 compared to the AM.

Displacements: Once the minor influence of the support of the short edges is established, it can be stated that NMT2 maintains the stiffness distribution of NMT0. In this way, it achieves a similar displacement response with an errorclearly below 10% on the maximum displacement and close to the 5% on the impact factor.

Accelerations: The mass of NMT2 is clearly reduced from NMT0, NMT1 or AM. It is well known that a reduction of the mass increases the acceleration level by the same amount on simple-degree-of-freedom systems (ERRI-D214-RP9-A 1999, ERRI-D214-RP9-N 1999, Carnerero 2007). In complex structural typologies, participation by a great number of vibration modes reduces this proportionality, but the tendency to increase the acceleration level with the mass reduction is still clear (Ugarte 2013). This explains differences of about 20% on the maximum acceleration of AM and NMT2.

NMT3 compared to the AM and to the NMT2.

Displacements: The transverse stiffness of NMT3 remains very similar to the stiffness of NMT0, NMT1, or AM. As displacements are mainly governed by low vibration modes whose generalized stiffness is determined by the transverse stiffness of the deck, the maximum dynamic displacement remains significantly unchanged, obtaining an error below 10%. The static displacement is determined by fewer vibration modes than the dynamic displacement, and it is affected more by the minor decrease of the generalized stiffness, which leads to a slight decrease of the impact factor (around 15%).

Accelerations: The mass and stiffness distribution on the central band is similar to the mass and stiffness distribution on AM, while the surface outside the central band has less influence than in NMT2. Hence, the obtained maximum acceleration is slightly higher but very similar to the one obtained on AM, maintaining an error below 5%. Nonetheless, it must be taken into account that the acceleration response is governed by higher vibration modes than the displacement behavior. The weight of the longitudinal stiffness over the global stiffness increases with the vibration modes, and thus the slab elimination outside the central band mainly affects the acceleration response. Although the acceleration level is approximately independent of stiffness variations (not completely, see Ugarte (2013), the resonant velocity is not, showing a decrease of around 10% on the resonant velocity of the maximum acceleration from AM to NMT3.

NMT4 compared to the AM and the NMT3.

Displacements: Because of reduced bending inertia of the transverse beams outside the central band, the transverse stiffness of the first vibration modes of NMT4 is slightly decreased compared to NMT3. Thus, the maximum displacement is increased, although it is not quite proportional (see Ugarte 2013). The particular amount of this increase depends on the specific characteristics and position of the central band over the deck. According to the results obtained, one can say that the influence of this phenomenon is limited for the usual deck width to central band width ratios, achieving in this case an increase of the maximum displacement from NMT3 to NMT4 of 7.23%.

As for NMT3, the static displacement tends to increase over the dynamic displacement, and thus the impact factor tends to decrease slightly in comparison to AM. For the usual pergola bridge deck width to central band width ratios, the impact factor is expected to remain similar to the one obtained for the NMT3, and so the error on the impact factor is estimated to remain below 15-20%. The reduction of stiffness of the first vibration modes also affects the resonant velocity of the maximum displacement, showing a reduction of about 15%.

Accelerations: Comparing AM and NMT4, we may observe the independence of the acceleration level to the stiffness variation, achieving an error on the maximum acceleration of less than 5% (as happened when comparing AM to NMT3). In spite of this, the reduction of stiffness is clearly patent on the reduction of resonant velocity of the maximum acceleration as well, obtaining an error that slightly exceeds 20%.

4. Conclusions

Throughout this paper, the authors propose a simple analytical model to study the dynamic behavior of pergola bridge decks. Also, this model is compared to the dynamic response of bi-dimensional FE models that represent the real distributions of mass and stiffness on this kind of structure. The following conclusions can be drawn:

1. The analytical model accurately represents the simplified structural reality that it represents, achieving an error on the main dynamic design parameters below or very similar to 5% when compared to an equivalent FE numerical model.
2. The influence of the support of the short edges is found to be negligible.
3. When it is compared to more complex numerical models that represent real alternatives of pergola bridge decks, the overall behavior of the analytical model is still very good, achieving errors below 5-10%. Nevertheless, in some specific cases the following considerations need to be made.
    a. For those decks of pergola bridges where the slab is uniformly distributed over the entire surface of the deck, a moderate increase of the maximum acceleration is expected. Its magnitude depends mainly on the ratio between the mass on the central band and the mass outside it, achieving values around 20% higher than those of the analytical model for the usual mass ratios.
    b. For those decks of pergola bridges where the slab is only defined on the central band along which the track is settled, a slight decrease of the impact factor is expected, achieving values around 15% lower than those of the analytical model.
    c. In these cases, special attention should be taken with the upper limit of the analyzed velocity range, as a reduction of 15-20% on the resonant velocity of both displacement and acceleration response is expected. Thus, for this kind of deck the recommendation is to increase the upper limit of the velocity range the same amount to obtain the expected resonant peaks in the analyzed range.

Taking into account these considerations, the analytical model proposed in this paper has been shown to be a simple and reliable methodology to develop usually complex and difficult-to-evaluate dynamic calculations. The analytical model allows structural engineers to make dynamically aware designs for pergola bridge decks, beginning in the early stages of the project. In this way, the structure can easily be dimensioned, employing more complex and time consuming numerical methods only as a verification tool at the final stages of the project.

References

Arenas, J.J. (1981), *Análisis de Tableros Rectos de Puente Mediante el Modelo de Losa Ortótropa*, Cátedra de Puentes. E.T.S. Ingenieros de Caminos, Santander.

Bruno, D., Greco, F. and Lonetti, P. (2008), "Dynamic impact analysis of long-span cable stayed bridges under moving loads", *Eng. Struct.*, **30**, 1160-1177.

Carnerero, A. (2007), *Comportamiento Dinámco de Tableros de Puentes de Ferrocarril de Alta Velocidad Formados con Elementos Transversales a la dirección de la vía*, Universidad Politécnica de Madrid, Madrid.

Carnerero, A., Ripa, T. and Iglesias, C. (2014), "Dynamic response of high-speed railway bridge decks with beams transverse to the direction of the track", *J. Bridge Eng.*, **19**(11), 04014047.

Clough, R.W. and Penzien, J. (1995), *Dynamics of Structures*, 3rd Edition, Computers & Structures, Berkeley.

Cusens, A.R. and Pama, R.P. (1975), *Bridge Deck Analysis*, John Wiley & Sons Ltd, London, New York.

EN 1991-2 (2003), Eurocode 1: Actions on structures-Part 2: Traffic loads on bridges, Brussels: CEN.

EN 1992-1-1 (2004), Eurocode 2: Design of concrete structures-Part 1-1: General rules and rules for buildings. s.l.:CEN.

ERRI-D214-RP9-A (1999), Ponts-rails pour vitesses > 200 km/h. Rapport final. Partie A. Synthèse des résultats des travaux de recherche du 214, s.l.: European Rail Research Institute (ERRI).

ERRI-D214-RP9-B (1999), Ponts-rails pour vitesses > 200 km/h. Rapport final. Partie B. Proposition de fiche UIC, s.l.: European Rail Research Institute (ERRI).

Frýba, L. (1999), *Vibration of Solids and Structures Under Moving Loads*, 3rd Edition, Thomas Telford Ltd., Prague.`

Gabaldón, F., Goicolea, J.M., Navarro, J.A., Riquelme, F. and Dominguez, I. (2004), *Dynamic analysis of hyperestatic structures under high speed train loads*, Congress Bridge High-Speed Railways, Porto.

Goicolea, J.M. (2007), *La consideración de los fenómenos dinámicos en el proyecto de puentes ferroviarios*, Córdoba, s.n., p. Sesión 4.

Hambly, E.C. (1991), *Bridge Deck Behaviour*, CRC Press, London.

Hillerborg, A. (1948), *A study of dynamic influences of moving loads on girders.* s.l., Preliminary Publication, 661-667.

I/SC/PS-OM/2298 (1997), *Sovraccarichi per il carolo dei ponti ferroviari. Instruzioni per la progettazione, l'esecuzione e il collaudo.*. s.l.:Ferrovie dello Stato.

IAPF-07 (2007), *Instrucción de acciones a considerar en puentes de ferrocarril*, Ministerio de Fomento, Madrid.

Ju, S.H. and Lin, H.T. (2003), "Numerical investigation of a steel arch bridge and interaction with high speed trains", *Eng. Struct.*, **25**(2), 241-250.

Lacarbonara, W. and Colone, V. (2007), "Dynamic response of arch bridges traversed by high-speed trains", *J. Sound Vib.*, **304**(1), 72-90.

Manterola, J. (1977), *Análisis de Tableros de Puentes por Métodos Armónicos*, Instituto Eduardo Torroja de la Construcción y del Cemento, Madrid.

Marchesiello, S., Fasana, A., Garibaldi, L. and Piombo, B.A.D. (1999), "Dynamics of multi-span continuous straight bridges subject to multi-degrees of freedom moving vehicle excitation", *J. Sound Vib.*, **224**(3), 541-561.

Martínez-Rodrigo, M.D., Lavado, J. and Museros, P. (2010), "Transverse vibrations in existing railway bridges under resonant conditions: Single-track versus double-track configurations", *Eng. Struct.*, **32**(7), 1861-1875.

Timoshenko, S.P. (1922), "On the forced vibration of bridges", *Philosophical Magazine Series 6*, **43**(257), 1018-1019.

Ugarte, J. (2013), *Análisis del Comportamiento Dinámico de Tableros de Puentes Pérgola de Ferrocarril en Líneas de Alta Velocidad*, Universidad Politécnica de Madrid (UPM), Madrid.

UIC (1979), UIC Code 776. s.l.: Union Internacional de Chemins de fer (UIC).

UIC, H. s. d. (2010), *High speed around the world. Maps*, Paris, s.n.

Willis, R. (1849), "Preliminary essay to the appendix B: Experiments for determining the effects produced by causing weights to travel over bars with different velocities", Report of the commissioners appointed to inquire into the application of iron to railway structures, W. Clowes and Sons, London.

Yang, Y.B., Yau, J.D. and Hsu, L.C. (1997), "Vibration of simple beams due to trains moving at high speeds", *Eng. Struct.*, **19**(11), 936-944.

Yau, J.D. and Yang, Y.B. (2004), "Vibration reduction for cable-stayed bridges travelled by high speed trains", *Finite Elem. Anal. Des.*, **40**(3), 341-359.

Zhu, X.Q. and Law, S.S. (2003), "Dynamic behavior of orthotropic rectangular plates under moving loads", *J. Eng. Mech.*, ASCE, **129**(1), 79-87.

PL

Notations

<u>*The following symbols are used in this paper:*</u>

a, b = longitudinal and transverse dimensions of a deck;
a_0, b_0 = longitudinal and transverse position of a singular point along the track;
$A_i(t)$, $B_i(t)$, $C_i(t)$, $D_i(t)$ = Temporal functions for the definition of the dynamic parameters of the deck;
$c(x, y)$ = damping coefficient;
d_k = distance between the first load of a train and the load P_k;
D_1, D_2 = longitudinal and transverse coupling unit stiffness of an orthotropic plate;
D_x, D_y = longitudinal and transverse flexural unit stiffness of an orthotropic plate;
D_{xy} , D_{yx} = longitudinal and transverse torsional unit stiffness of an orthotropic plate;
e = slab thickness;
E_{slab}, E_{beam} = elasticity modulus;
G_{slab}, G_{beam} = shear modulus;
h = time step length utilised for the step-by-step integration method on the numerical analysis;
$I_{x,0}$, $I_{y,0}$ = flexural stiffness of longitudinal and transverse beams;
J_x, J_y = torsional stiffness of longitudinal and transverse beams;
k = number of certain load of a train;
K_r^* = generalized stiffness of vibration mode r;
KP = number of the last load of a train;
$m(x, y)$ = mass per unit area of an orthotropic plate;
n , m = number of longitudinal and transverse half sin waves of the modal form of an orthotropic plate;
$p(x, y, t)$ = load at position x, y and instant t;
P, P_k = load of a single axis;
$P1_r$, $P2_r$, $P3_r$, $P4_r$, PF_r, PR_r = fictitious harmonic load functions for the definition of the generalized load of vibration mode r;
P_r^* = generalized load of vibration mode r;
r = number of the vibration mode of an orthotropic plate;
R = number of the highest vibration mode considered in the analysis;
s = position coordinate along the direction of the track;
s_x, s_y = longitudinal spacing between transverse beams and viceversa;
t = time;
t_k = time between the origin and the entrance of the load P_k on the deck;
v = train velocity;
$v(x, y, t)$ = vertical displacement of an orthotropic plate;
w_r= circular frequency of vibration mode r;
w_{D_r}= circular damped frequency of vibration mode r;
$w_{Pi,r}$ = circular frequency of the fictitious harmonic load function Pi_r;
x, y = longitudinal and transverse position coordinates;
$\beta_{1,r}$, $\beta_{2,r}$ = frequency ratio for fictitious loads $P1_r$ and $P3_r$, and $P2_r$ and $P4_r$ respectively;
Δt = time that needs a single load to cross the deck at certain constant velocity v;
θ = angle between the direction of the track and the longitudinal direction;
θ_{crit} = θ angle for which the track enters the deck over its corner;
ν = poisson's coefficient;
ξ_r = damping ratio of vibration mode r;
$\varphi_{Pi,r}$ = phase angle of the fictitious harmonic load function Pi_r;
$\phi_r(x, y)$ = modal shape at position x, y for vibration mode r;
$2H$ = torsional and coupled unit stiffness of an orthotropic plate;

Appendix A

Definition of the circular frequency and the phase angle of the 4 harmonic loads that form the generalized load of a single load moving over an orthotropic plate

Comparing Eqs. (18), (19) and (23), the circular frequency and phase angle of loads $P1_r$ and $P2_r$ can directly be obtained.

$$w_{P1,r} = v \cdot \pi \cdot \left(\frac{n}{a} \cdot \cos\theta - \frac{m}{b}\sin\theta\right) \tag{A.1}$$

$$w_{P2,r} = v \cdot \pi \cdot \left(\frac{n}{a} \cdot \cos\theta + \frac{m}{b}\sin\theta\right) \tag{A.2}$$

$$\varphi_{P1,r} = \frac{n\cdot\pi}{a} \cdot \left(a_0 - \frac{b_0}{\tan\theta}\right) \cdot H(\theta - \theta_{crit}) - \frac{m\cdot\pi}{b} \cdot (b_0 - a_0 \cdot \tan\theta) \cdot H(\theta_{crit} - \theta) + \frac{\pi}{2} \tag{A.3}$$

$$\varphi_{P2,r} = \frac{n\cdot\pi}{a} \cdot \left(a_0 - \frac{b_0}{\tan\theta}\right) \cdot H(\theta - \theta_{crit}) + \frac{m\cdot\pi}{b} \cdot (b_0 - a_0 \cdot \tan\theta) \cdot H(\theta_{crit} - \theta) + \frac{\pi}{2} \tag{A.4}$$

Therefore, taking into account that the circular frequency of the two harmonic functions of the rear load has to be equal to that of the two harmonic functions of the front load, the rear load can be obtained solely by defining the right phase angle for its harmonics

$$w_{P3,r} = w_{P1,r} \tag{A.5}$$

$$w_{P4,r} = w_{P2,r} \tag{A.6}$$

$$\varphi_{P3,r} = \varphi_{P1,r} + w_{p1,r} \cdot \Delta t + \pi \tag{A.7}$$

$$\varphi_{P4,r} = \varphi_{P2,r} + w_{p2,r} \cdot \Delta t + \pi \tag{A.8}$$

Appendix B

Definition of the temporal functions for Eq. (25)

$$A_{rk}(t) = A_{1,rk}(t) + A_{2,rk}(t) \tag{B.1}$$

$$A_{1,rk}(t) = \left(1 - \beta_{1,r}{}^2\right) \cdot \sin\left(w_{P1,r} \cdot (t - t_k) + \varphi_{P1,r}\right) -2 \cdot \xi_r \cdot \beta_{1,r} \cdot \cos\left(w_{P1,r} \cdot (t - t_k) + \varphi_{P1,r}\right) \tag{B.2}$$

$$A_{2,rk}(t) = e^{-\xi_r \cdot w_r \cdot (t - t_k)} \cdot \left[\left(2 \cdot \xi_r \cdot \beta_{1,r} \cdot \cos\left(\varphi_{P1,r}\right) - \left(1 - \beta_{1,r}{}^2\right) \cdot \sin\left(\varphi_{P1,r}\right)\right) \cdot \cos\left(w_{D_r} \cdot (t - t_k)\right) + \frac{\beta_{1,r}}{\sqrt{1 - \xi_r{}^2}} \cdot \left[\left(2 \cdot \xi_r{}^2 + \beta_{1,r}{}^2 - 1\right) \cdot \cos\left(\varphi_{P1,r}\right) + \left(\xi_r \cdot \left(\frac{\beta_{1,r}{}^2 - 1}{\beta_{1,r}}\right) - 2 \cdot \xi_r \cdot \beta_{1,r}\right) \cdot \sin\left(\varphi_{P1,r}\right) \cdot \sin\left(w_{D_r} \cdot (t - t_k)\right)\right] \tag{B.3}$$

$$B_{rk}(t) = B_{1,rk}(t) + B_{2,rk}(t) \tag{B.4}$$

$$B_{1,rk}(t) = \left(1 - \beta_{2,r}{}^2\right) \cdot \sin\left(w_{P2,r} \cdot (t - t_k) + \varphi_{P2,r}\right) -2 \cdot \xi_r \cdot \beta_{2,r} \cdot \cos\left(w_{P2,r} \cdot (t - t_k) + \varphi_{P2,r}\right) \tag{B.5}$$

$$B_{2,rk}(t) = e^{-\xi_r \cdot w_r \cdot (t - t_k)} \cdot \left[\left(2 \cdot \xi_r \cdot \beta_{2,r} \cdot \cos\left(\varphi_{P2,r}\right) - \left(1 - \beta_{2,r}{}^2\right) \cdot \sin\left(\varphi_{P2,r}\right)\right) \cdot \cos\left(w_{D_r} \cdot (t - t_k)\right) + \frac{\beta_{2,r}}{\sqrt{1 - \xi_r{}^2}} \cdot \left[\left(2 \cdot \xi_r{}^2 + \beta_{2,r}{}^2 - 1\right) \cdot \cos\left(\varphi_{P2,r}\right) + \left(\xi_r \cdot \left(\frac{\beta_{2,r}{}^2 - 1}{\beta_{2,r}}\right) - 2 \cdot \xi_r \cdot \beta_{2,r}\right) \cdot \sin\left(\varphi_{P2,r}\right)\right] \cdot \sin\left(w_{D_r} \cdot (t - t_k)\right)\right] \tag{B.6}$$

$$C_{rk}(t) = C_{1,rk}(t) + C_{2,rk}(t) \tag{B.7}$$

$$C_{1,rk}(t) = \left(1 - \beta_{1,r}{}^2\right) \cdot \sin\left(w_{P3,r} \cdot (t - t_k - \Delta t) + \varphi_{P3,r}\right) -2 \cdot \xi_r \cdot \beta_{1,r} \cdot \cos\left(w_{P3,r} \cdot (t - t_k - \Delta t) + \varphi_{P3,r}\right) \tag{B.8}$$

$$C_{2,rk}(t) = e^{-\xi_r \cdot w_r \cdot (t - t_k - \Delta t)} \cdot \left[\left(2 \cdot \xi_r \cdot \beta_{1,r} \cdot \cos\left(\varphi_{P3,r}\right) - \left(1 - \beta_{1,r}{}^2\right) \cdot \sin\left(\varphi_{P3,r}\right)\right) \cdot \cos\left(w_{D_r} \cdot (t - t_k - \Delta t)\right) + \frac{\beta_{1,r}}{\sqrt{1 - \xi_r{}^2}} \cdot \left[\left(2 \cdot \xi_r{}^2 + \beta_{1,r}{}^2 - 1\right) \cdot \cos\left(\varphi_{P3,r}\right) + \left(\xi_r \cdot \left(\frac{\beta_{1,r}{}^2 - 1}{\beta_{1,r}}\right) - 2 \cdot \xi_r \cdot \beta_{1,r}\right) \cdot \sin\left(\varphi_{P3,r}\right)\right] \cdot \sin\left(w_{D_r} \cdot (t - t_k - \Delta t)\right)\right] \tag{B.9}$$

$$D_{rk}(t) = D_{1,rk}(t) + D_{2,rk}(t) \tag{B.10}$$

$$D_{1,rk}(t) = \left(1 - \beta_{2,r}{}^2\right) \cdot \sin\left(w_{P4,r} \cdot (t - t_k - \Delta t) + \varphi_{P4,r}\right) \; 2 \cdot \xi_r \cdot \beta_{2,r} \cdot \cos\left(w_{P4,r} \cdot (t - t_k - \Delta t) + \varphi_{P4,r}\right) \tag{B.11}$$

$$D_{2,rk}(t) = e^{-\xi_r \cdot w_r \cdot (t - t_k - \Delta t)} \cdot \left[\left(2 \cdot \xi_r \cdot \beta_{2,r} \cdot \cos\left(\varphi_{P4,r}\right) - \left(1 - \beta_{2,r}{}^2\right) \cdot \sin\left(\varphi_{P4,r}\right)\right) \cdot \cos\left(w_{D_r} \cdot (t - t_k - \Delta t)\right) + \frac{\beta_{2,r}}{\sqrt{1 - \xi_r{}^2}} \cdot \left[\left(2 \cdot \xi_r{}^2 + \beta_{2,r}{}^2 - 1\right) \cdot \cos\left(\varphi_{P4,r}\right) + \left(\xi_r \cdot \left(\frac{\beta_{2,r}{}^2 - 1}{\beta_{2,r}}\right) - 2 \cdot \xi_r \cdot \beta_{2,r}\right) \cdot \sin\left(\varphi_{P4,r}\right)\right] \cdot \sin\left(w_{D_r} \cdot (t - t_k - \Delta t)\right)\right] \tag{B.12}$$